Theoretical description of the Fano effect in the angle-integrated valence-band photoemission of paramagnetic solids

J. Minár and H. Ebert
Department Chemie, Physikalische Chemie, Universität München, Butenandtstraße 5-13, D-81377 München, Germany

G. Ghiringhelli,* O. Tjernberg,† and N. B. Brookes
European Synchrotron Radiation Facility, Boîte Postale 220, 38043 Grenoble Cedex, France

L. H. Tjeng
Solid State Physics Laboratory, Materials Science Centre, University of Groningen, Nijenborgh 4, 9747 AG Groningen, The Netherlands
(Received 28 July 2000; revised manuscript received 11 January 2001; published 21 March 2001)

A theoretical description of the Fano effect in the angle-integrated valence-band photoemission of paramagnetic solids is presented that is based on the one-step model of photoemission and relativistic multiple-scattering theory. Applications to fcc-Cu led to a very satisfying agreement with recent experimental data that show the Fano effect, i.e., a finite spin-polarization for the spectra is found for excitation with circularly polarized radiation. As can be demonstrated by model calculations, this finding is caused by the presence of spin-orbit coupling. To allow for a more detailed discussion of the spectra a simplified description of the Fano effect is presented that treats spin-orbit coupling as a perturbation.

DOI: 10.1103/PhysRevB.63.144421 PACS number(s): 75.20.En, 71.15.Rf, 71.20.Be, 71.70.Ej

I. INTRODUCTION

Recently there has been much interest in experiments based on magnetic circular dichroism as a tool to study the electronic structure of magnetic materials.[1,2] Without doubt the most prominent example for this is the magnetic circular dichroism in x-ray absorption (MCXD) that allows us to probe in an element specific way the spin and orbital magnetic moments of the absorber atom by making use of the so-called sum rules.[3–6] In the case of photoemission, circular dichroism has also been extensively investigated for core levels[7,8] as well as the valence band.[7,9–11] In discussing their first MCXD spectra, recorded at the Fe *K* edge, Schütz *et al.*[12] pointed out that the magnetic dichroism can be traced back to the Fano effect, i.e., the creation of spin-polarized electrons in an excited state when circularly polarized radiation is used for excitation. For paramagnetic—this means in the present context not spontaneously spin-polarized—solids the spin polarization of the excited electron is just reversed if the helicity of the radiation is reversed. For ferromagnetic solids, on the other hand, this does not apply any more because of the spin-dependent electronic structure and as a consequence magnetic circular dichroism is observed.

Originally, the Fano effect was predicted by Fano[13,14] to occur for free atoms as a consequence of spin-orbit coupling and the selection rules connected with circularly polarized radiation. This was demonstrated by Heinzmann *et al.* for free Cs atoms[15] and also for poly-crystalline Cs films.[16] Later on, the Fano effect, that is sometimes called optical spin orientation, was observed in many different systems such as semiconductors and adsorbates.[17,18] A corresponding theoretical description for the experiment on paramagnetic solids was presented by Koyama and Merz[19] on the basis of the three-step model of photoemission. Later theoretical work[20,21] was based on the more advanced one-step model that does not have to rely on an artificial decomposition of the photoemission process into three distinct steps. Corresponding theoretical investigations provided a rather detailed and accurate description of the available spectroscopic data stemming from angle-resolved valence-band photoemission measurements on single crystals. In particular it allowed to explain the observation of a spin polarized photo electron current for linearly polarized light and low-symmetry surfaces. A survey of the theoretical description of spin-polarization effects in the angle-resolved photoemission from nonmagnetic solids has been given recently by Feder and Henk.[22] The corresponding experimental investigations have been reviewed by Schneider and Kischner.[23]

In this paper we provide a detailed analysis of the Fano effect in the valence-band photoemission of paramagnetic solids, based on the one-step model of photoemission and relativistic multiple-scattering theory. By dealing with the multiple-scattering process in real space, we have a very simple expression for the *k*-integrated spin resolved valence-band photoemission spectra, with which we can make accurate quantitative comparison with recent spin resolved circularly polarized data of polycrystalline Cu metal by Ghiringhelli *et al.*[24] To discuss the resulting spectra in some detail, we perform model calculations by treating the spin-orbit coupling as a perturbation, thereby arriving at a very transparent explanation for the observed spin polarization.

II. THEORETICAL FRAMEWORK

A. Fully relativistic calculation of the photo current

As mentioned above a rather sophisticated fully relativistic description of spin and angle-resolved photoemission has been developed during the last years by several groups.[20,21,25,26] This is based on the one-step model and represents the electronic Green's function by making use of the multiple scattering or Korringa-Kohn-Rostoker (KKR) formalism. By dealing with the multiple-scattering problem in real space, a very simple expression could be derived by

Ebert and Schwitalla[26] for the spin resolved and angle-integrated valence-band photoemission spectra of ferromagnetic solids.

Making use of the single-scatterer approximation, i.e., ignoring multiple-scattering events for the final state the resulting photocurrent with energy E' and spin character m_s is given in the case of one atom per unit cell by

$$
\begin{aligned}
&I(E,m_s;\omega,\vec{q},\lambda)\\
&\propto \mathrm{Im} \sum_{\Lambda\Lambda''\mu=\mu''} C_{\Lambda}^{-m_s} C_{\Lambda''}^{-m_s} \Bigg\{ \sum_{\Lambda_1\Lambda_2} \tau^{00}_{\Lambda_1\Lambda_2}(E)\\
&\times \Bigg[\sum_{\Lambda'} t^0_{\Lambda'\Lambda}(E') M^{\vec{q}\lambda}_{\Lambda'\Lambda_1} \Bigg] \Bigg[\sum_{\Lambda'''} t^0_{\Lambda'''\Lambda''}(E') M^{\vec{q}\lambda}_{\Lambda'''\Lambda_2} \Bigg]^*\\
&- \sum_{\Lambda'\Lambda'''\Lambda_1} t^0_{\Lambda'\Lambda}(E') I^{\vec{q}\lambda}_{\Lambda'\Lambda_1\Lambda'''} t^{0*}_{\Lambda'''\Lambda''}(E') \Bigg\}, \qquad (1)
\end{aligned}
$$

where ω, $\vec{q}$, and λ specify the energy, wave vector, and polarization of the radiation and $E=E'-\omega$ is the energy of the initial states. The quantities $C_{\Lambda}^{m_s}$ are Clebsch-Gordon coefficients with the index $\Lambda=(\kappa,\mu)$ combining the relativistic spin orbit and magnetic quantum numbers.[27] The electronic structure of the system is represented by the single site t matrix $t^n_{\Lambda\Lambda'}(E)$ and the scattering path operator $\tau^{nm}_{\Lambda\Lambda'}(E)$ connecting lattice sites at $\vec{R}_n$ and $\vec{R}_m$. The corresponding matrix elements $M^{\vec{q}\lambda}_{\Lambda\Lambda'}$ and $I^{q\lambda}_{\Lambda\Lambda'\Lambda''}$ are given by[26]

$$
M^{\vec{q}\lambda}_{\Lambda\Lambda'} = \int d^3r [TZ_{\Lambda}(\vec{r},E')]^{\times} X_{\vec{q}\lambda}(\vec{r}) Z_{\Lambda'}(\vec{r},E) \qquad (2)
$$

and

$$
\begin{aligned}
I^{\vec{q}\lambda}_{\Lambda\Lambda'\Lambda''} = \int d^3r \int d^3r' [TZ_{\Lambda}(\vec{r},E')]^{\times} X_{\vec{q}\lambda}(\vec{r})\\
\times Z_{\Lambda'}(\vec{r}_<,E) J^{\times}_{\Lambda'}(\vec{r}_>,E) X^{\times}_{\vec{q}\lambda}(\vec{r}') [TZ_{\Lambda''}(\vec{r}'),E')]. \qquad (3)
\end{aligned}
$$

Here $Z_{\Lambda}(\vec{r},E)$ and $J_{\Lambda}(\vec{r},E)$ are the regular and irregular solutions to the Dirac equation, $X_{\vec{q},\lambda}(\vec{r}) = -e\vec{\alpha}\cdot\vec{A}_{\vec{q}\lambda}$ represents the interaction of the electrons and the radiation with $\vec{\alpha}$ the vector of Dirac-matrices and $\vec{A}_{\vec{q}\lambda}$ the vector potential representing the radiation field.[27] Finally, $T=-i\sigma_y K$ is the time reversal operator. Equation (1) can be used straightforwardly to calculate the spin-resolved photocurrent $I(E,m_s;\omega,\vec{q},\lambda)$ if circularly polarized radiation is used. This will be denoted in short $I^{m_s}_{\lambda}$ in the following with $m_s=\uparrow(\downarrow)$ and $\lambda=+(-)$ for left and right circularly polarized radiation.

To compare the resulting theoretical spectra with experiment (see the next section) various intrinsic and experimental broadening mechanisms have to be accounted for. To represent the various life time effects a Lorentzian broadening has been applied with an energy-dependent width $\Gamma(E)$ $=0.01+0.02(E-E_F)^2$ eV with E_F the Fermi energy. A Gaussian broadening has been added afterwards using σ $=0.4$ eV.

B. Perturbational treatment of spin-orbit coupling

The scheme sketched above that is based on the four-component Dirac formalism deals with all relativistic effects in a rigorous way. This means in particular that the effects of spin orbit coupling are properly accounted for. On the other hand it is not very transparent and does not allow for a simple interpretation of the resulting spectra. To overcome this problem a simpler scheme is introduced in the following.

The fully relativistic scheme has been derived in analogy to the nonrelativistic photoemission theory worked out by Durham.[28] Starting point of his approach is the following expression for the photocurrent:

$$
\begin{aligned}
&I(E,\vec{k},m_s;\omega,\vec{q},\lambda)\\
&\propto \int d^3r_1 \int d^3r_2 \phi^{\mathrm{final}}_{\vec{k}m_s}(\vec{r}_1,E')^{\dagger}\\
&\times X_{\vec{q}\lambda}(\vec{r}_1) \mathrm{Im}\, \underline{\underline{G}}(\vec{r}_1,\vec{r}_2,E) X^{\times}_{\vec{q}\lambda}(\vec{r}_2) \phi^{\mathrm{final}}_{\vec{k}m_s}(\vec{r}_2,E'). \qquad (4)
\end{aligned}
$$

Here the initial valence-band states are represented by the Green's function $\underline{\underline{G}}(\vec{r},\vec{r}',E)$ and the final state $\phi^{\mathrm{final}}_{\vec{k}m_s}(\vec{r},E')$ is assumed to be a time reversed low-energy electron-diffraction state. Originally this expression was meant to deal with nonmagnetic solids and the influence of spin-orbit coupling was ignored in addition. These restrictions can be overcome by working in a two-component formalism; i.e., the wave functions are set up as spinors and $\underline{\underline{G}}(\vec{r},\vec{r}',E)$ is a 2×2 matrix with respect to the spin index m_s. The spin-orbit coupling is treated as a perturbation in the following. In particular it is assumed that it influences only the initial states represented by the Green's function $\underline{\underline{G}}(\vec{r},\vec{r}',E)$ but not the final states $\phi^{\mathrm{final}}_{\vec{k}m_s}(\vec{r},E')$ at relatively high energy E'. In line with this, spin-orbit induced spin flip transitions are ignored for the electron-photon interaction operator $X_{\vec{q}\lambda}(\vec{r})$.

Representing the final states using multiple-scattering theory and using the single-scatterer approximation, one arrives for the spin-resolved and angle-integrated photocurrent at

$$
\begin{aligned}
I^{m_s}_{\lambda} = \sum_L [t_l(E')]^2 \int d^3r \int d^3r' Z_l(r,E') Y^*_L(\hat{r}) \chi^{\dagger}_{m_s} X_{\vec{q}\lambda}(\vec{r})\\
\times \mathrm{Im}\, \underline{\underline{G}}(\vec{r},\vec{r}',E) X^{\dagger}_{\vec{q}\lambda}(\vec{r}') Z_l(r',E') Y_L(\hat{r}') \chi_{m_s}. \qquad (5)
\end{aligned}
$$

Here $t_l(E)$, and $Z_l(r,E)Y_L(\hat{r})\chi_{m_s}$ are the l-dependent single site t matrix and radial wave function for the final state, $Y_L(\hat{r})$ is a spherical harmonic with $L=(l,m_l)$ and χ_{m_s} is a spinor with spin character m_s. Because spin-orbit coupling

for the final state as well as spin-flip transitions are ignored only the diagonal elements of the Green's-function matrix enter the above expression.

The influence of spin-orbit coupling for the valence-band states can be accounted for by representing it by a corresponding perturbation operator $\hat{H}_{SOC}=\xi(\vec{r})\vec{l}\vec{\sigma}$ (Ref. 27) leading for the 2×2 Green's-function matrix $\underline{\underline{G}}$ to

$$\underline{\underline{G}}=\underline{\underline{G}}^0+\underline{\underline{G}}^0\hat{H}_{SOC}\underline{\underline{G}}^0+\underline{\underline{G}}^0\hat{H}_{SOC}\underline{\underline{G}}^0\hat{H}_{SOC}\underline{\underline{G}}^0+\ldots, \quad (6)$$

with all arguments suppressed. Here

$$\underline{\underline{G}}^0(\vec{r},\vec{r}',E)=\begin{pmatrix} G^0(\vec{r},\vec{r}',E) & 0 \\ 0 & G^0(\vec{r},\vec{r}',E)\end{pmatrix} \quad (7)$$

is the Green's function for the unperturbated solid for which the two spin components are identical. On the basis of the model calculations to be presented below, it is obvious that it is completely sufficient to stop the above expansion after the second term; i.e., to treat $\hat{H}_{SOC}$ only in first order. Because only the spin-diagonal elements of $\underline{\underline{G}}(\vec{r},\vec{r}',E)$ enter the above expression for $I_\lambda^{m_s}$ it follows immediately that only the spin diagonal part $H_{SOC}^{dia}=\xi(r)l_z\sigma_z$ of the spin-orbit interaction operator $\hat{H}_{SOC}$ has to be considered. The expansion in Eq. (6) can be dealt with by representing the Green's function $G^0(\vec{r},\vec{r}',E)$ within the framework of nonrelativistic multiple-scattering theory:

$$\begin{aligned}\underline{\underline{G}}(\vec{r},\vec{r}',E)=&\sum_{L,L',m_s} Z_l(r,E)Y_L(\hat{r})\chi_{m_s}\tau_{LL'}^{nm}(E)Z_{l'}(r',E)\\ &\times Y_{L'}^*(\hat{r})\chi_{m_s}^\dagger-\sum_L Z_l(r_<,E)Y_L(\hat{r})\chi_{m_s}\\ &\times J_l(r_>,E)Y_L^*(\hat{r}')\chi_{m_s}^\dagger\delta_{nm}, \end{aligned}\quad (8)$$

where $Z_l(r,E)$ and $J_l(r,E)$ are the regular and irregular solutions to the radial Schrödinger equation with angular momentum character l. The quantity $\tau_{LL'}^{nm}(E)$ is the corresponding scattering path operator that—as for the wave functions—does not depend on the spin character m_s.

The various products in Eq. (8) imply an integration over the whole space. For the following qualitative discussion it is, however, completely sufficient to restrict the influence of spin-orbit coupling operator $\hat{H}_{SOC}^{dia}$ to the central atomic site for which the absorption process takes place. For the same reason and for the sake of clearness terms connected with the irregular solutions $J_l(r,E)$ will be dropped in the following. With these simplifications the photocurrent can be written as

$$\begin{aligned}I_\lambda^{m_s}\propto&\sum_L[t_l(E)]^2\sum_{L_1L_2}\Big\{M_{Lm_sL_1m_s}^\lambda M_{Lm_sL_2m_s}^{\lambda *}\mathrm{Im}\,\tau_{L_1L_2}(E)\\ &+\sum_{L_3L_4}M_{Lm_sL_1m_s}^\lambda M_{L_2m_sL_3m_s}^{SOC}M_{LL_4}^{\lambda *}\\ &\times\mathrm{Im}[\tau_{L_1L_2}(E)\tau_{L_3L_4}(E)]\Big\}, \end{aligned}\quad (9)$$

where the site index for the site-diagonal scattering operators $\tau_{LL'}$ have been suppressed. In Eq. (9)

$$\begin{aligned}M_{Lm_sL'm_s'}^\lambda=&\int d^3rZ_l(r)Y_L^*(\hat{r})\chi_{m_s}^\dagger X_{\vec{q}\lambda}(\vec{r})Z_{l'}(r)Y_{L'}(\hat{r})\chi_{m_s'}\\ =&R_{ll'}\sqrt{\frac{4\pi}{3}}\lambda(-1)^m[(2l+1)(2l'+1)]^{1/2}\\ &\times\begin{pmatrix} l & 1 & l' \\ 0 & 0 & 0\end{pmatrix}\begin{pmatrix} l & 1 & l' \\ -m & \lambda & m'\end{pmatrix}\delta_{m_sm_s'}\end{aligned}\quad (10)$$

is a matrix element of the nonrelativistic electron-photon interaction operator $X_{\vec{q}\lambda}$ that has been used here in its configuration form $X_{\vec{q}\lambda}(\vec{r})\propto\vec{r}\cdot\vec{A}_{\vec{q}\lambda}$. The Wigner $3j$ symbols

$$\begin{pmatrix} l & 1 & l' \\ -m & \lambda & m'\end{pmatrix}$$

immediately imply for circularly polarized radiation ($\lambda=\pm1$) the selection rules $l-l'=\pm1$, $m_l-m_{l'}=\lambda$ and $m_s-m_s'=0$. For the spin-orbit coupling operator $\hat{H}_{SOC}^{dia}$ one has the corresponding matrix elements

$$\begin{aligned}M_{Lm_sL'm_s'}^{SOC}=&\int d^3rZ_l(r)Y_l^*(\hat{r})\chi_{m_s}^\dagger\hat{H}_{SOC}^{dia}(\vec{r})Z_{l'}(r)Y_{L'}(\hat{r})\chi_{m_s'}\\ =&\xi_lm_lm_s\delta_{ll'}\delta_{m_lm_l'}\delta_{m_sm_s'},\end{aligned}\quad (11)$$

with ξ_l the radial part of the matrix element. Restricting the involved valence-band states to have d character; i.e., by setting $l_1=l_2=l_4=2$, one finally arrives at the rather simple expression for the photocurrent:

$$\begin{aligned}I_\lambda^{m_s}=&\sum_l 5\frac{4\pi}{3}(\overline{R_{l_2}})^2(2l+1)\\ &\times\begin{pmatrix} l & 1 & 2 \\ 0 & 0 & 0\end{pmatrix}^2\sum_{m_1}\begin{pmatrix} l & 1 & 2 \\ -m & \lambda & m_1\end{pmatrix}^2\\ &\times\sum_{m_2}[N_2\,\mathrm{Im}\,\tau_{2m_12m_2}+\overline{\xi_l}m_2m_sN_2^2\\ &\times\mathrm{Im}(\tau_{2m_12m_2}\tau_{2m_22m_1})].\end{aligned}\quad (12)$$

For the discussion following below we have introduced the overlap integral $N_2=\int r^2dr[Z_2(r)]^2$ for the d electrons and used the corresponding normalized radial matrix elements $\overline{R_{l_2}}=R_{l_2}/\sqrt{N_2}$ and $\overline{\xi_2}=\xi_2/N_2$, respectively.

III. RESULTS AND DISCUSSION

The relativistic approach sketched in the previous section has been applied so far only to deal with a number of ferromagnetic binary alloy systems.[26,29] For these systems it has been predicted that even for the angle-integrated mode there should occur in general a magnetic circular dichroism. While for the spin-integrated spectra the dichroism should be rather small in general, it should be quite pronounced for the spin-resolved case. Application of the approach to paramagnetic solids is of course possible without modifications and allows

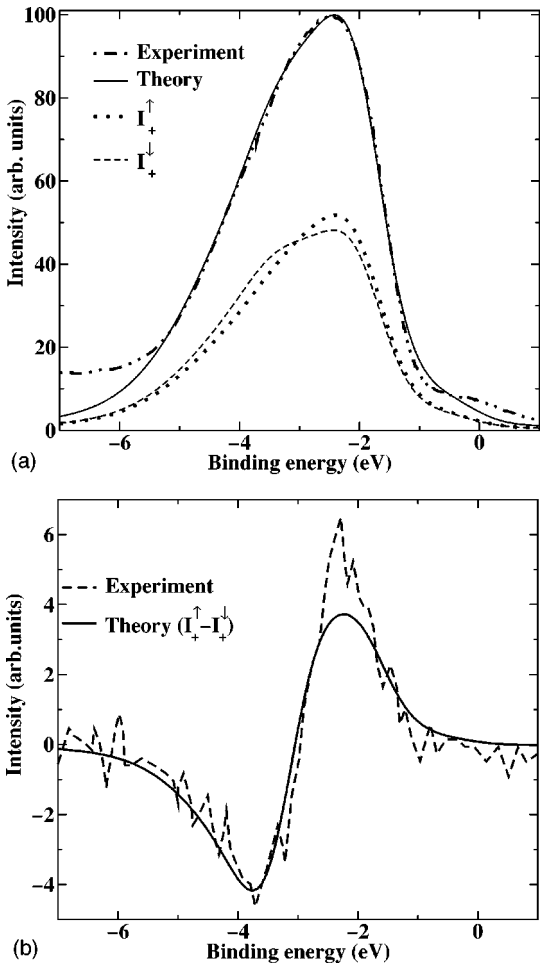

FIG. 1. Top: spin and angle-integrated VB-XPS spectrum of fcc Cu for a photon energy of 600 eV. Bottom: spin difference $\Delta I_+ = I_+^\uparrow - I_+^\downarrow$ of the photocurrent for excitation with left circularly polarized radiation. Theory: full line; experiment: dashed line (Ref. 24). The upper panel shows in addition the theoretical spin-resolved spectra $I_+^{\uparrow(\downarrow)}$.

in particular to study the Fano effect without additional contributions to the spin polarization of the photocurrent due to an intrinsic exchange splitting. The top panel of Fig. 1 shows corresponding results for the spin- and angle-integrated valence band x-ray photoemission (VB-XPS) spectra of pure fcc Cu for a photon energy of 600 eV together with corresponding experimental data.

Obviously, the width and shape of the main peak connected with the Cu *d* band is reproduced by the calculations in a very satisfying way. However, one should also note that there are some deviations around the Fermi energy and that there is an appreciable secondary electron background contribution to the experimental spectrum for higher binding energies. In Fig. 1 the spin-resolved spectra $I_+^{m_s}$ for excitation with left circularly polarized radiation ($\lambda = +1$) have been added. These spectra already show that one has a small but finite spin difference $\Delta I_+ = I_+^\uparrow - I_+^\downarrow$ throughout the region of the *d*-band complex that changes sign with increasing binding energy. The main features of the spin difference ΔI_+ can be seen more clearly in the lower panel of Fig. 1. This figure shows in particular that the spin difference amounts to about

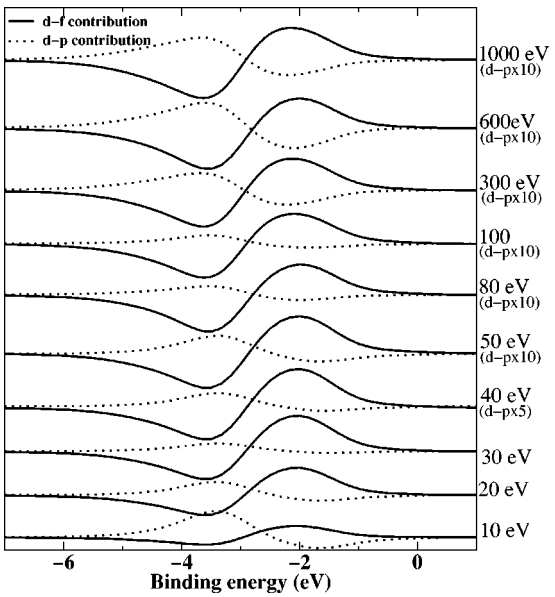

FIG. 2. Decomposition of the theoretical spin difference of the photocurrent $\Delta I_+ = I_+^\uparrow - I_+^\downarrow$ according to the angular momentum character of the initial and final states for various photon energies. Only the dominating *d-p* and *d-f* contributions are shown. For photon energies $\geqslant 40$ eV the *d-p* contributions have been scaled up by a factor of 5 or 10, respectively.

5% (the same normalization has been used for both figures). Comparison with the corresponding experimental spin difference ΔI_+ shows that this is reproduced in a quantitative way by the fully relativistic calculations. The rather good agreement obviously opens the way to a detailed discussion of the experimental spectra by a corresponding analysis of the theoretical results.

The expression for the photocurrent $I_\lambda^{m_s}$ given in Eq. (1) of course allows a straightforward decomposition according to the angular momentum character of the final state. Because the main features of the spectra shown in Fig. 1 are connected with the *d* states and because of the dipole approximation used for the matrix elements $M_{\Lambda\Lambda'}^\lambda$ [see Eq. (1)] only *d-p* and *d-f* contributions to the difference spectra ΔI_+ have to been considered. The results in Fig. 2 clearly show that the *d-p* and *d-f* contributions are of opposite sign for all photon energies. For a photon energy of about 15 eV both contributions are of the same order of magnitude and for this reason should more or less cancel one another. [For calculations of the spectra for low photon energies, multiple-scattering events for final states have been accounted for by replacing the single site *t* matrix $t_{\Lambda\Lambda'}(E')$ in Eq. (1) with the corresponding site-diagonal scattering path operator $\tau_{\Lambda\Lambda'}(E')$.[29] For photon energies higher than 50 eV this does not influence the spectra, i.e., use of the single-scattering approximation is well justified.] With increasing photon energy the relative weight of the *d-p* contribution to ΔI_+ drops rapidly and above about 50 eV it contributes in general less than 10%. Within a nonrelativistic description of the VB-XPS experiment there would be no spin difference at all even for excitation with circularly polarized radiation. This is because the spin-resolved spectra $I_\lambda^{m_s}$ are in this case unam-

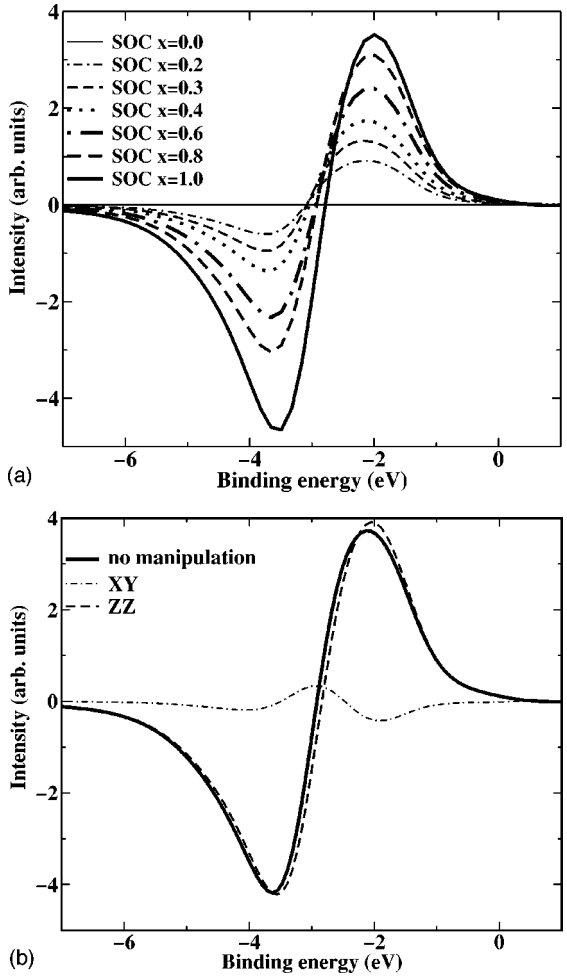

FIG. 3. The theoretical results for the spin difference ΔI_+ obtained by model calculations. Top: the strength of the spin orbit coupling x_ξ has been varied between 0 and 1. Bottom: only the spin-diagonal (zz) and only the spin-mixing (xy), respectively, part of the full spin-orbit coupling (SOC) has been kept for the calculations.

biguously connected with the two spin subsystems with spin character m_s and because these have identical photoemission cross sections (see below). This simple situation completely changes if spin-orbit coupling is considered in addition.

To investigate the mechanism giving rise to the spin difference ΔI_+ two types of model calculations have been performed that were done in a relativistic way but with the spin-orbit coupling manipulated. In a first set of calculations the relative strength of the spin-orbit coupling x_ξ was varied between 0 and 1 (the value 0 corresponds to the so-called scalar-relativistic situation without spin-orbit coupling while 1 represents the situation according to the Dirac equation). As can be seen from Fig. 3 the shape of the spin difference ΔI_+ hardly changes with the strength of the spin-orbit coupling x_ξ and the amplitude increases more or less linearly with x_ξ. This clearly demonstrates that the Fano effect is a first-order effect with respect to the spin-orbit coupling. In a second set of calculations the strength of the spin-orbit coupling was unchanged $(x_\xi=1)$ but the spin-orbit coupling was split into a part that is diagonal with respect to the spin $(\propto l_z\sigma_z)$,[30] and a part that gives rise to a hybridization of the spin systems $[\propto(l_x\sigma_x+l_y\sigma_y)]$.[31] Keeping only the first part, i.e., suppressing the second spin-mixing part, leads to a spin difference ΔI_+ that is nearly unchanged as it can be seen in the lower panel of Fig. 3. If the second part is kept instead, the spin difference ΔI_+ is rather small and its sign is reversed with respect to the original curve. These results are in full accordance with the variation of ΔI_+ if the strength of the spin-orbit coupling is varied. As it can be demonstrated on the basis of the formalism presented in Sec. II B ΔI_+ is caused only by the spin-diagonal part of the spin-orbit coupling operator if it is accounted for to first order. The spin-mixing part, on the other hand, contributes only if it is accounted for to higher order. Although the first-order contribution to ΔI_+ is obviously by far dominating, the spectra in Fig. 3 clearly show several features that have to be ascribed to higher-order contributions; in the upper panel, the amplitude of ΔI_+ does not vary strictly linearly with x_ξ, the zero position at around 3-eV binding energy slightly shifts with x_ξ, and in the lower panel, ΔI_+ does not vanish if only the spin-mixing part of the spin-orbit coupling is kept in the calculations.

The formalism presented in Sec. II B that treats spin-orbit coupling as a perturbation allows us to give a rather simple explanation for the results shown in Figs. 1–3. The first term N_2 Im $\tau_{2m_1 2m_2}$ in the square brackets of Eq. (12) stems from the unperturbed system represented by Green's function G^0. Because it can be identified with a contribution to the *d*-like density of states, one arrives at the usual point of view: in the XPS regime, for which multiple scattering in the final state can be ignored, the photoemission spectrum maps the matrix element weighted density of states of the conduction band. Furthermore, one notes that this contribution to $I_\lambda^{m_s}$ does not depend on the spin character m_s. This implies that there will be no spin difference $\Delta I_\lambda = I_\lambda^\uparrow - I_\lambda^\downarrow$ whatever polarization λ is used. In contrast to this, the last term in Eq. (12) is directly proportional to m_s and as a consequence a finite spin difference ΔI_λ may occur. This means in particular that the Fano effect is indeed a first-order effect with respect to the spin-orbit coupling $\hat{H}_{SOC}$ as it was indicated by the model calculations (see top panel of Fig. 3). If the spin-orbit coupling is ignored for the final states this implies automatically that only the spin-diagonal part $\hat{H}_{SOC}^{dia}$ of the full operator $\hat{H}_{SOC}$ has to be considered. Again this is in line with the results of the model calculations presented in Fig. 3 that indicated that the spin mixing part of the spin orbit coupling operator is less important than the spin diagonal part and contributes only as a higher-order correction. These results make clear that the observed spin difference ΔI_λ, properly normalized with respect to the total intensity I_λ, can be seen as a rather direct measure for the spin-orbit coupling strength ξ. Consequently, one may expect, for example, for Au a spin difference ΔI_λ, that is, according to the ratio of the spin-orbit energy splittings ΔE_{SOC} of the *d*-electrons $[\Delta E_{SOC}(\mathrm{Cu}) = 0.271$ eV, $\Delta E_{SOC}(\mathrm{Au}) = 1.415$ eV], about a factor of 5.2 higher than for Cu. (Instead of ξ we used here ΔE_{SOC} defined by the difference in the resonance energies of the $d_{5/2}$ and $d_{3/2}$ phase shifts δ_j, because this quantity does not depend on energy; see below.) However, it should be noted that for Au higher-order contributions to ΔI_λ might get impor-

tant, as it is indicated by the results shown in Fig. 3 (bottom) connected with the spin mixing (xy) part of the full spin-orbit coupling operator $\hat{H}_{SOC}$. Finally, it should be emphasized that the use of the ΔI_λ spectrum to determine the spin-orbit coupling parameter ξ will give only an average value over the occupied part of the valence band. However, ξ derived from the radial wave function $R_{l=2}(r,E)$ may vary by a factor of 2 within that region. In addition ξ derived from the spin-orbit splitting seen in the dispersion relation $E(\vec{k})$ depends on the wave vector $\vec{k}$ as well.[32] This is clearly demonstrated by experimental data derived from angle-resolved photoemission experiments.[33]

To allow for a more detailed discussion based on Eqs. (12) we exploited the cubic symmetry of the system studied here. Using complex spherical harmonics $Y_L(\hat{r})$ as basis functions in Eqs. (5) and (8) this implies for the d block of the τ matrix the form

$$\tau = \begin{pmatrix} c & & & & c \\ & a & & & \\ & & b & & \\ & & & a & \\ c & & & & c \end{pmatrix}, \tag{13}$$

with $c=(a+b)/2$ and a and b giving rise to the t_{2g}- and e_g-like density of states, respectively. This results in the relation

$$\begin{aligned} 5(2l+1)&\begin{pmatrix} l & 1 & 2 \\ 0 & 0 & 0 \end{pmatrix}^2 \sum_{m_1} \begin{pmatrix} l & 1 & 2 \\ -m & \lambda & m_1 \end{pmatrix}^2 \\ &\times \sum_{m_2} m_2 \,\mathrm{Im}(\tau_{2m_1 2m_2} \tau_{2m_2 2m_1}) \\ &= S_{l\lambda}\,\mathrm{Im}\left(\frac{a(4b+a)}{25}\right). \end{aligned} \tag{14}$$

For left circularly polarized radiation ($\lambda=+1$) the sign $S_{l\lambda}$ is $+1$ for final states with p character ($l=1$) and -1 for a final states with f character ($l=3$). This means that the different sign for the d-p and d-f contributions to ΔI_+ (see Fig. 2) is simply a consequence of the different weights for $l=1$ and $l=3$, respectively, occurring in the summations over the spin quantum number m_2 in Eq. (14) (m_2 runs from -2 to $+2$ while all other proceeding terms are positive). Because for a given polarization λ the terms in Eq. (14) for final p and f states differ only in sign, the resulting spin difference ΔI_+ and its energy dependence shown in Fig. 2 stems from the very different energy dependence of the radial matrix elements R_{12} and R_{32} [see Eq. (10)] for p- and f-like final states, respectively. If right circularly polarized radiation ($\lambda=-1$) is assumed, the sign $S_{l\lambda}$ is just reversed; i.e., one has $S_{l(-1)}=-S_{l(+1)}$. This implies for the spin-resolved photocurrents $I_\lambda^{m_s}$ the relationship $I_+^\uparrow = I_-^\downarrow$ and $I_+^\downarrow = I_-^\uparrow$. In particular one has for the spin difference $\Delta I_+ = -\Delta I_-$. This means in particular that there is of course no circular dichroism present.

Finally, one can make use of the identity $\partial G/\partial E = -GG$ for the Green's function to interpret the right-hand side of Eq. (14). Ignoring the difference in the density of states $n(E)$ with t_{2g} and e_g character this expression is simply proportional to the energy derivative of the density of states $n(E)$. This simple explanation is obviously in line with the theoretical spectra shown in Fig. 1. As one can see ΔI_+ has a zero at the maximum position of $I_+ = \Delta I_+^\uparrow + \Delta I_+^\downarrow$ that in turn essentially maps $n(E)$. In addition the asymmetry of ΔI_+ is in full accordance with that of I_+. Calculations for paramagnetic bcc Fe and fcc Au supported the conclusion that the spin-orbit induced spin difference ΔI_+ essentially maps the energy derivative of the density of states $n(E)$. However, for these two cases no full correspondence for all details of the more structured ΔI_+ and $dn(E)/dE$ curves could be found. Presumably this is because the difference between the t_{2g} and e_g projected density of states cannot be ignored anymore.

IV. SUMMARY

Results of fully relativistic calculations for the valence-band photoemission spectra of fcc Cu using circularly polarized radiation have been presented. These were found to reproduce recent experimental data in a very satisfying way. In particular the spin-orbit induced spin difference ΔI_λ was found in very good agreement with experiment. As already observed earlier it turned out that multiple-scattering effects are important only for photon energies below about 50 eV. The use of the single-scatter approximation is therefore well justified at higher energies. Analysis of the theoretical spectra revealed, that for very low photon energies the d-p contribution dominates the spin difference ΔI_λ, while for photon energies higher than about 50 eV the d-f contribution represent about 90% of the effect. Because both contributions differ in their sign ΔI_λ changes sign when the photon energy increases. Model calculations performed in addition clearly demonstrated the role of the spin-orbit coupling. In particular they revealed that the Fano effect in the angle-integrated VB-XPS is a first-order effect and the spin mixing part of the spin-orbit coupling operator should normally play a minor role. All these findings could be explained in a very transparent way by extending Durham's scheme to deal with photoemission by treating spin-orbit coupling as a perturbation. In addition it could be demonstrated that the spin-orbit induced spin difference ΔI_λ essentially reflect the energy derivative of the density of states $n(E)$ of the system. From the results presented one can immediately conclude that for heavier elements with a stronger spin orbit coupling a more pronounced spin-difference ΔI_λ has to be observed. This implies that spin resolved and angle-integrated valence-band photoemission can be used as a rather simple and sensitive probe to determine the average spin-orbit coupling strength for the valence-band electrons. It should be applicable for this propose even for multidomain ferromagnets that show no net magnetization.

ACKNOWLEDGMENT

This work was funded by the BMBF (Bundesministerium für Bildung und Forschung) within the program *Zirkular polarisierte Synchrotronstrahlung: Dichroismus, Magnetismus und Spinorientierung* under contract 05 SC8WMA 7.

*Present address: Dipartimento di Fisica, Politecnico di Milano, piazza Leonardo da Vinci 32, 20133 Milano, Italy.

†Present address: Material Physics, KTH, S-100 44 Stockholm, Sweden.

[1] *Core Level Spectroscopies for Magnetic Phenomena: Theory and Experiment*, edited by P. S. Bagus, G. Pacchioni, and F. Parmigiani (Plenum, New York, 1995).

[2] *Spin-Orbit Influenced Spectroscopies of Magnetic Solids*, Lecture Notes in Physics Vol. 466, edited by H. Ebert and G. Schütz (Springer, Berlin, 1996).

[3] R. Wienke, G. Schütz, and H. Ebert, J. Appl. Phys. **69**, 6147 (1991).

[4] B. T. Thole, P. Carra, F. Sette, and G. van der Laan, Phys. Rev. Lett. **68**, 1943 (1992).

[5] G. Schütz, M. Knülle, and H. Ebert, Phys. Scr. **T49**, 302 (1993).

[6] P. Carra, B. T. Thole, M. Altarelli, and X. Wang, Phys. Rev. Lett. **70**, 694 (1993).

[7] H. B. Rose, C. Roth, F. U. Hillebrecht, and E. Kisker, Solid State Commun. **91**, 129 (1994).

[8] L. Baumgarten, C. M. Schneider, H. Petersen, F. Schäfers, and J. Kirschner, Phys. Rev. Lett. **65**, 492 (1990).

[9] C. M. Schneider, P. Schuster, M. S. Hammond, and J. Kirschner, Europhys. Lett. **16**, 689 (1991).

[10] J. Bansmann, C. Westphal, G. Getzlaff, F. Fegel, and G. Schönhense, J. Magn. Magn. Mater. **104**, 1691 (1992).

[11] A. Rampe, D. Hartmann, and G. Güntherodt, in *Spin-Orbit Influenced Spectroscopies of Magnetic Solids*, Lecture Notes in Physics Vol. 466 (Ref. 2), p. 49.

[12] G. Schütz, W. Wagner, W. Wilhelm, P. Kienle, R. Zeller, R. Frahm, and G. Materlik, Phys. Rev. Lett. **58**, 737 (1987).

[13] U. Fano, Phys. Rev. **184**, 250 (1969).

[14] U. Fano, Phys. Rev. **178**, 131 (1969).

[15] U. Heinzmann, J. Kessler, and J. Lorenz, Z. Phys. **240**, 42 (1970).

[16] U. Heinzmann, K. Jost, J. Kessler, and B. Ohnemus, Z. Phys. **251**, 354 (1972).

[17] F. Meier, in *Polarized Electrons in Surface Physics*, edited by R. Feder (World Scientific, Singapore, 1985), Chap. 10.

[18] U. Heinzmann and G. Schonhense, in *Polarized Electrons in Surface Physics* (Ref. 17), Chap. 11.

[19] K. Koyama and H. Merz, Z. Phys. B **20**, 131 (1975).

[20] B. Ackermann and R. Feder, J. Phys. C **18**, 1093 (1985).

[21] B. Ginatempo, P. J. Durham, B. L. Gyorffy, and W. M. Temmerman, Phys. Rev. Lett. **54**, 1581 (1985).

[22] R. Feder and J. Henk, in *Spin-Orbit Influenced Spectroscopies of Magnetic Solids*, Lecture Notes in Physics Vol. 466 (Ref. 2), p. 85.

[23] C. M. Schneider and J. Kischner, Crit. Rev. Solid State Mater. Sci. **20**, 179 (1995).

[24] G. Ghiringhelli, N. B. Brookes, O. Tjernberg, and L. H. Tjeng (unpublished).

[25] M. Fluchtmann, J. Braun, and G. Borstel, Phys. Rev. B **52**, 9564 (1995).

[26] H. Ebert and J. Schwitalla, Phys. Rev. B **55**, 3100 (1997).

[27] M. E. Rose, *Relativistic Electron Theory* (Wiley, New York, 1961).

[28] P. J. Durham, J. Phys. F: Met. Phys. **11**, 2475 (1981).

[29] S. Ostanin and H. Ebert, Phys. Rev. B **58**, 11 577 (1998).

[30] H. Ebert, H. Freyer, A. Vernes, and G.-Y. Guo, Phys. Rev. B **53**, 7721 (1996).

[31] H. Ebert, H. Freyer, and M. Deng, Phys. Rev. B **56**, 9454 (1997).

[32] H. Eckardt, L. Fritsche, and J. Noffke, J. Phys. F: Met. Phys. **14**, 97 (1984).

[33] P. L. Wincott, N. B. Brookes, D. S. L. Law, and G. Thornton, Phys. Rev. B **33**, 4373 (1986).